

Surface-Reactive Patchy Nanoparticles and Nanodiscs Prepared by Tandem Nanoprecipitation and Internal Phase Separation

Divya Varadharajan, Hatice Turgut, Joerg Lahann, Hiroshi Yabu,* and Guillaume Delaittre*

Nanoparticles with structural or chemical anisotropy are promising materials in domains as diverse as cellular delivery, photonic materials, or interfacial engineering. The surface chemistry may play a major role in some of these contexts. Introducing reactivity into such polymeric nanomaterials is thus of great potential, yet is still a concept in its infancy. In the current contribution, a simple nanoprecipitation technique leads to nanoparticles with diameters as low as 150 nm and well-defined reactive surface patches of less than 30 nm in width, as well as surface-reactive flat, disc-like nanoparticles with corresponding dimensions, via an additional crosslinking/delamination sequence. To this aim, chemically doped block copolymers (BCPs) are employed. Control over morphology is attained by tuning preparation conditions, such as polymer concentration, solvent mixture composition, and blending with non-functional BCP. Surface reactivity is demonstrated using a modular ligation method for the site-selective immobilization of thiol molecules. The current approach constitutes a straightforward methodology requiring minimal engineering to produce nanoparticles with confined surface reactivity and/or shape anisotropy.

self-assembly towards obtaining arbitrary features with smaller domain sizes, only recent studies have indicated that solution self-assembly of BCPs can also produce several complex nanostructured nanoparticles with domain sizes in the sub-50 nm range.^[1–5] In the process of internal phase separation of BCPs in colloidal 3D confinements, various morphologies can be obtained, e.g., Janus,^[6,7] lamellae,^[2,8–11] cylinder,^[12] or dot patterns.^[13–15] Beyond the vibrant field of supracolloidal assembly,^[16,17] such internally structured nanoparticles may find interesting applications at the monomeric level, for their bulk multicompartiment-based nature (e.g., as nanoreactors, nanocontainers for controlled release) as well as for their topographical or chemical surface heterogeneities, leading to their designation as patchy nanoparticles.^[18–21] Besides the most common Janus nanoparticles, whose main

1. Introduction


Towards bridging the structural control gap between structures found in nature and simpler man-made micro- and nanomaterials, significant advances have been made using the bottom-up approach of block copolymer (BCP) self-assembly. While remarkable progress has been achieved in bulk BCP

peculiarity lies in their interfacial properties, high-order internal structuration may be useful for mimicking natural phenomena or for interacting in a more efficient way with biological systems. For the former case, an example is the controlled docking of specific complementary enzymes on defined patches that can lead to enhanced cascade reactions due to a proximity effect, as found in metabolons.^[22] For the latter case, it is for instance

D. Varadharajan, Dr. H. Turgut, Dr. G. Delaittre
Institute of Toxicology and Genetics (ITG)
Karlsruhe Institute of Technology (KIT)
Hermann-von-Helmholtz-Platz 1, 76344 Eggenstein-Leopoldshafen, Germany
E-mail: guillaume.delaittre@kit.edu

D. Varadharajan, Dr. H. Turgut, Dr. G. Delaittre
Institute for Chemical Technology and Polymer Chemistry (ITCP)
Karlsruhe Institute of Technology (KIT)
Engesserstrasse 18, 76131 Karlsruhe, Germany

Prof. J. Lahann
Chemical Engineering
Materials Science and Engineering
Biomedical Engineering, and Macromolecular Science and Engineering
University of Michigan
Ann Arbor, MI 48109, USA

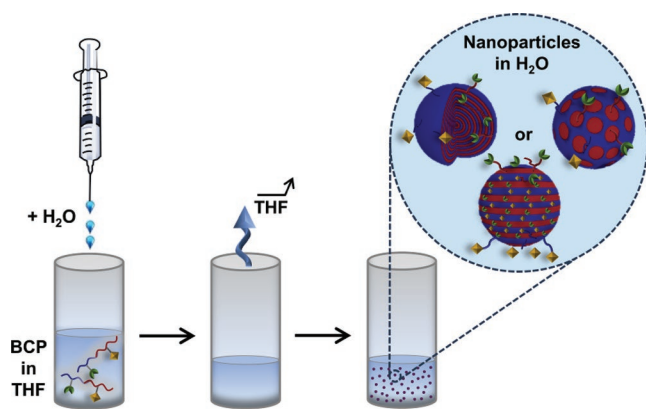
 The ORCID identification number(s) for the author(s) of this article can be found under <https://doi.org/10.1002/adfm.201800846>.

Prof. J. Lahann
Biointerfaces Institute
B26, Rm. 133S, 2800 Plymouth Road, Ann Arbor, MI 48109, USA

Prof. J. Lahann
Institute of Functional Interfaces (IFG)
Karlsruhe Institute of Technology (KIT)
Hermann-von-Helmholtz-Platz 1
76344 Eggenstein-Leopoldshafen, Germany

Prof. H. Yabu
WPI-Advanced Institute for Materials Research (AIMR)
Tohoku University
2-1-1, Katahira, Aoba-Ku, Sendai 980-8577, Japan
E-mail: yabu@tagen.tohoku.ac.jp

DOI: 10.1002/adfm.201800846



Scheme 1. Strategy developed in the present work to fabricate patchy nanoparticles with surface-expressed reactive groups by nanoprecipitation of functional BCPs, here PS-*b*-PI.

recognized that specific surface features may play a role in the cellular uptake of nanoparticles, quite probably in the same way viruses work.^[23–26] Although such patchy nanoparticles have been in existence, the currently available synthetic BCP nanoparticles that bear high spatial and structural control are by-and-large restricted to polymers^[8,27,28] and blends^[29] that are devoid of functionality. For example, Robb et al. described the use of self-assembled nanoparticles from post-modified poly(allyl glycidyl ether)-*b*-polylactide as modular delivery vehicles.^[30] Very recently, Hiraï et al. reported the preparation of virus-like particles using an asymmetric polystyrene-*b*-poly(*t*-butyl acrylate) BCP^[31] and Schmidt et al. that of reactive ellipsoidal striped nanoparticles from polystyrene-*b*-poly(2-vinylpyridine) BCP blended with analogue functional homopolymers.^[32]

Here, considering the great potential of functional patchy BCP nanoparticles, we study the evolution and control of phase separation morphologies during the process of nanoparticle formation by a simple nanoprecipitation method previously termed as *self-organized precipitation* (SORP, see **Scheme 1**),^[33] for a small library of structurally identical polystyrene-*b*-polyisoprene (PS-*b*-PI), which differ only by the nature of a small fraction of functional groups introduced in the PS segment. We tackle various aspects that affect the morphology of phase separation: (i) the synthetic strategy used to synthesize the polymer, (ii) the mole fraction and nature of the functional groups incorporated, and (iii) conditions used for the preparation of nanoparticles to acquire tailored morphologies and sizes (solvent, concentration, and blending). We find that besides the influence of functional groups—even in low amounts—the polymer end group exerts a major influence on the morphology of phase separation of the nanoparticles leading to various internal structures, such as spheres-in-matrix, onion-like, lamellae, as well as intermediate structures. We then focus on obtaining striped spherical particles that have domain sizes in the 15–30 nm, which could potentially be used for multistep enzyme cascade reactions or as biological particle mimics for enhanced cell uptake, as mentioned above. We demonstrate the accessibility of surface-reactive groups for domain-specific decoration, as well as the generation of surface-reactive anisotropic daughter nanoparticles, i.e., nanodiscs, by post-nanoprecipitation selective crosslinking and delamination.

2. Results and Discussion

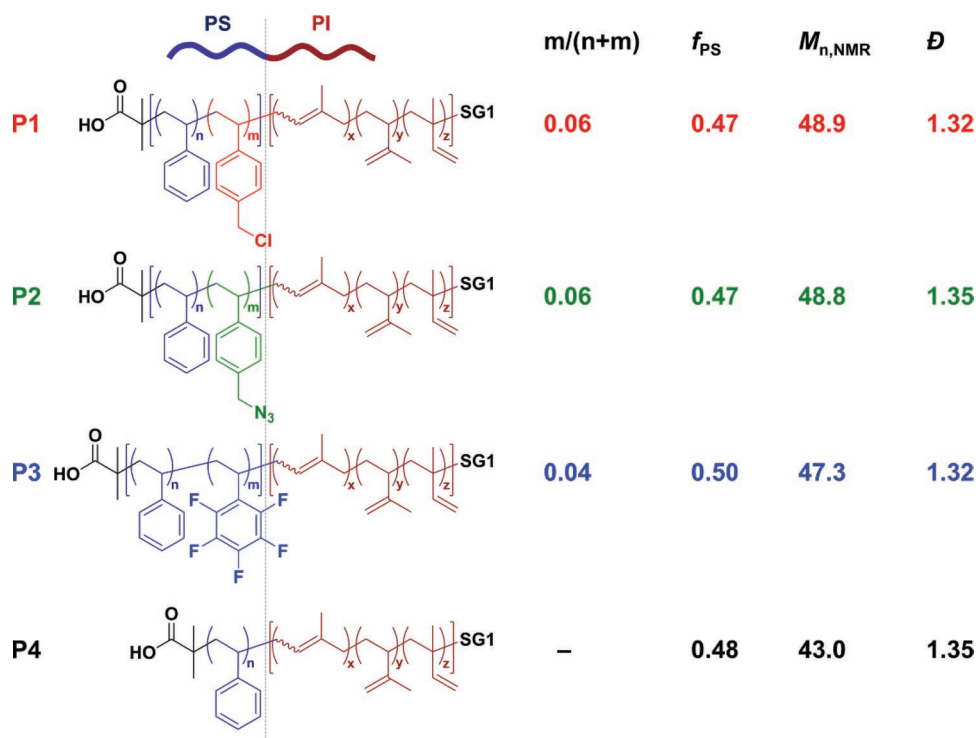
2.1. Choice of the Block Copolymer System

The PS-*b*-PI BCP scaffold was chosen for two reasons. First and foremost, this is the first system which has been shown to yield nanoparticles with internal nanostructuring by SORP.^[33] Secondly, we recently pioneered SG1 nitroxide-mediated polymerization (NMP) as a straightforward route for the synthesis of functional PS-*b*-PI with reasonable dispersity.^[34] Using NMP permits to avoid traditional, yet more complicated and less functional group-tolerant protocols based on ionic polymerization and post-polymerization modification. A small set of PS-*b*-PI BCPs is here developed and includes halide (**P1**), azide (**P2**), and pentafluorophenylalkyl (**P3**) moieties in the PS block (**Scheme 2**). The selected functional comonomers were chosen such that they structurally resemble the PS backbone as much as possible, yet introduce reactivity later available at the surface of the nanoparticles for precise molecular immobilization. For a description of the experimental procedures, please refer to the Supporting Information. A schematic representation and the characteristics of the polymers can be seen in **Scheme S1**, **Figures S1** and **S2**, and **Tables S1** and **S2** in the Supporting Information, respectively.

For a BCP in the melt, equal volume fractions of the blocks are well known to lead to lamellar phase separation in the solid state.^[35] Therefore, the volume fractions of our PS and PI blocks are close to 0.5 because we eventually aim at obtaining internal structuration with unidirectionally stacked lamellae. The targeted molar masses of the functional BCPs were ca. 50 kg mol⁻¹ as we ultimately sought to obtain domain sizes in the sub-50 nm range, which is relevant for biomimetics applications (e.g., synthetic metabolons and virus-like particles). Such precise patterns with domain sizes of ca. 10–50 nm can be used further for patterned immobilization of specific biomolecules for potential applications in the fields of drug delivery,^[36] photonics,^[37,38] biosensing,^[39,40] among others. The amount of functional groups in the PS block was kept rather low (<10 mol%) so as to impart functionality, while presumably not perturbing the phase separation behavior of the original PS-*b*-PI scaffold. This is based on our observations of a similar set of BCPs, which revealed that in the solid state these BCPs lead to lamellar morphologies with only minor changes in the interlamellar distance.^[34]

2.2. Hydrodynamic Diameters of the BCP Nanoparticles

Nanoparticles were prepared by a simple nanoprecipitation method, previously termed SORP. It typically involves the use of a good solvent to molecularly dissolve the BCP. Then, a miscible non-solvent of both blocks is added (typically water), leading to the formation of nanoparticles. Within these nanoparticles, the BCP eventually is in the solid state after evaporation of the good solvent and the two blocks phase separate. Note that in this technique, both segments are excluded of the continuous phase (i.e., water), as opposed to classic nanoprecipitation of amphiphilic diblock copolymers. Here, tetrahydrofuran (THF) was used as the good solvent owing to its suitability to dissolve



Scheme 2. Structure and characteristics of the PS-*b*-PI BCPs synthesized and utilized for the current study. f_{PS} is the volume fraction of the PS block. $M_{n,NMR}$ is the number-averaged molar mass determined by a combination of SEC and NMR. \bar{D} is the dispersity value determined by SEC. The ternary molar ratio of isomeric isoprene units $x:y:z$ is typically equal to 0.80:0.13:0.07.

both PS and PI segments, its miscibility with water, and its volatility. As expected, the incorporation of a small amount of functional monomers in the PS block of **P1–3** did not alter the overall solubility in THF. However, the concentration of the polymer solution and the mixing ratio of good solvent to non-solvent were found to exert an influence on particle size (see below). For potential applications, we were interested to reach an average particle size of $\approx 150\text{--}300$ nm as it usually offers a good compromise between high surface area and good processability (e.g., separation by centrifugation). In addition, this size range permits the co-existence of several repeating patterns with a period of ca. 30–50 nm within the same particle.

In general, the process of formation of nanoparticles is based on the principle of nucleation, where the BCPs are first dissolved in a good solvent and an increase in the amount of non-solvent causes the compact folding of polymer chains into small nuclei.^[41] The sizes of the particles formed are further governed by the concentration of the polymer solution and the solubility of both blocks of the BCP in the THF/water mixture. During the formation of nanoparticles, THF was gradually allowed to evaporate, and that in turn decreased the solubility of the hydrophobic BCPs. As it is already known that the hydrodynamic diameters of non-functional PS-*b*-PI influences the internal phase-separated structures of the nanoparticles,^[6,28] we herein conducted a brief study focusing on the size dependence of nanoparticles made of functional BCPs **P1–3**.

Different preparation conditions were evaluated for each BCP (see **Figure 1**, and Table S3 and Figures S3–S5, Supporting Information): two initial polymer concentrations in THF

(0.1 and 1.0 mg mL⁻¹) and three THF:water ratios (1:3, 1:1, and 3:1 vol/vol). In each case, particle size was measured both by dynamic light scattering (DLS) and by transmission electron microscopy (TEM, using statistical analysis). Four main trends are emerging: (i) first, all nanoparticles prepared with a THF-to-water content of 1:3 vol/vol are within the same hydrodynamic diameter regime, with most of them in the 150–250 nm range, irrespective of the polymer concentration (see **Figure 1** at 25 vol% THF and Table S3, Entries 1, 4, 7, 10, 13, and 16, Supporting Information). (ii) Within the range of current conditions, the polymer concentration does not seem to have a marked impact on the hydrodynamic diameters. (iii) The hydrodynamic diameters for nanoparticles prepared from BCPs with chloromethylphenyl (**P1**) and pentafluorophenyl (**P3**) functionalities are rather insensitive to preparation conditions, within the studied range. (iv) BCP **P2**, with azidomethylphenyl functionality, behaves very differently from **P1** and **P3** during nanoprecipitation. Indeed, while nanoparticles prepared from the latter BCPs remain within the same size domain under all studied conditions, nanoparticles prepared with **P2** undergo a significant size increase with increasing THF content to actually reach the micrometer range at THF:water ratios of 1:1 and 3:1 vol/vol. The particle size distribution obtained by statistical analysis of electron micrographs (≈ 100 particles for each sample) matches roughly the number-based distributions obtained by DLS for BCPs **P1** and **P3** (Figures S3 and S5, Supporting Information). As expected for these more polydisperse samples with large diameters, deviations can however be seen in the case of **P2** (**Figure S4**, Supporting Information). Nevertheless, it can

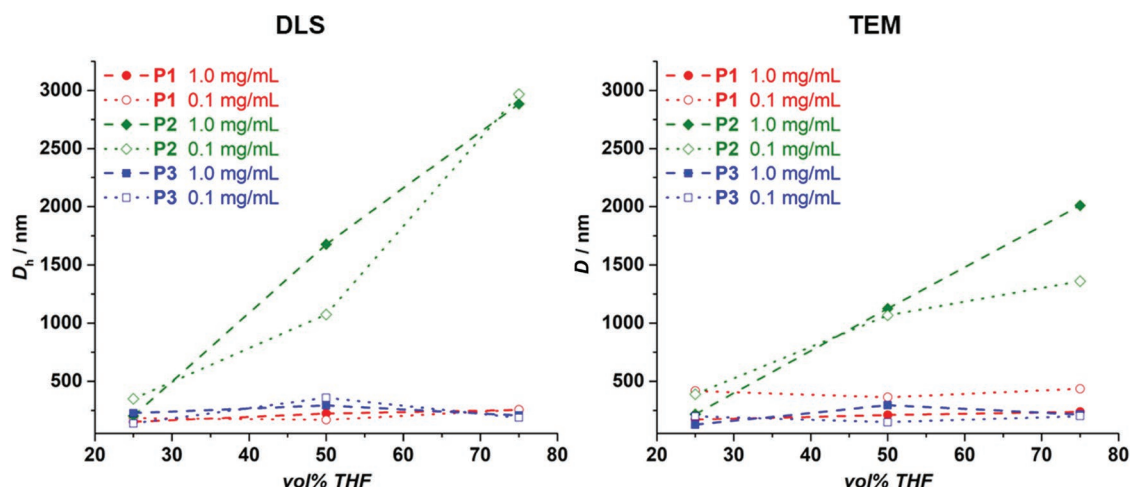


Figure 1. Evolution of the intensity-average hydrodynamic diameters measured by DLS (left) and of the diameters measured by TEM for nanoparticles obtained by nanoprecipitation with increasing THF content prepared from BCPs P1–3 at different polymer concentrations (0.1 and 1 mg mL⁻¹). Note that DLS measurements were performed after full evaporation of THF.

clearly be seen that the overall trends of particle size evolution are similar whether the latter is assessed by DLS or TEM (Figure 1).

The nature of the functional comonomers may explain such a behavior. Since the particles are formed via a nucleation-and-growth process during THF evaporation,^[41] an increasing THF content, i.e., an extended evaporation time of THF, should lead to larger particles. On the contrary, when a low THF content is used during nanoprecipitation, that is, a large amount of non-solvent, the polymer chains should quickly collapse, thereby creating a large number of nuclei and consequently smaller particles. This is for instance the case of P3, which possesses the most hydrophobic type of functional moiety (pentafluorophenylalkyl). However, P2 possesses rather polar azide moieties (dipoles), which may retard chain collapse by having a relatively higher affinity towards both water and THF. Hence, only a small number of nuclei are formed and the particles grow to a larger size as THF evaporates.

In any case, it is possible to obtain nanoparticles within the desired size range for all functional polymers by working with the appropriate conditions. The next step was to study the internal phase separation and the related surface patterns which interest us.

2.3. Morphological Study of the Internally Phase-Separated BCP Nanoparticles

The internal phase separation structures were observed using TEM or STEM after reacting the nanoparticles with an aqueous solution of osmium tetroxide (OsO₄). OsO₄ chemically crosslinks the double bonds present in the PI block and its corresponding phases in a selective manner. The presence of a heavy metal in the PI-containing domains advantageously leads to contrast in electron microscopy. In the present study, all classic TEM pictures were acquired in bright field (BF) mode, while scanning TEM (STEM) pictures were obtained in dark field (DF) mode. Therefore, in the TEM images, dark and

bright regions represent the PI and PS blocks, respectively, and vice versa in STEM images. At 0.1 mg mL⁻¹ (Figure 2, columns (A–F)1 and (A–F)3), all nanoparticles internally phase separate to form stacked lamellae structures (i.e., striped particles), onion-like particles, or intermediate morphologies which we term “T” as they correspond to states of transformation between two well-defined structures. An increase in concentration to 1 mg mL⁻¹ leads to clear onion-like structures in a majority of cases, e.g., for all P3 and P4 nanoparticles (Figure 2, (D–F)2 and (D–F)4), as well as “T” structures between onion-like and stacked lamellae (Figure 2, B4 and C4). In addition, internal spherical morphologies are also observed (Figure 2, A2 and B2).

The morphology of phase separation is governed by the Flory–Huggins interaction parameter between the two blocks, the solubility parameters (SPs) of the respective blocks, the volume fractions of the polymer segments (*f*), as well as the effect of 3D confinement of the polymeric chains at the nanoscale.^[28,42,43] As the SPs of both PS and PI are similar,^[44] their precipitation rates should be similar upon addition of water during nanoprecipitation. One would therefore expect this to result in simultaneous precipitation of both segments, leading to morphologies containing both PS and PI at the surface, at least in some well-defined conditions of concentration, temperature, and good solvent/non-solvent ratio. This is the case for PS-*b*-PI BCPs, which are devoid of functional moieties able to alter SPs.^[28] Clearly, with the currently considered BCPs P1–3, chloromethyl, azidomethyl, and fluorine substituents play an important role since they lead to different morphologies in identical conditions, as seen in Figure 2. A previous study by Li et al. describes the effect of selective solvent that swells specific polymer domains and alters the effective volume fraction ratio and curvature between polymer segments, thereby inducing morphological changes.^[45] It can be postulated that the presence of the functional groups do induce a modification of the swelling behavior of the PS phase with THF. Based on the pseudo phase diagram represented in Figure 2, the concentration of polymer as well as the amount of THF can significantly affect the morphologies. It can be seen that various defined morphologies finally leading

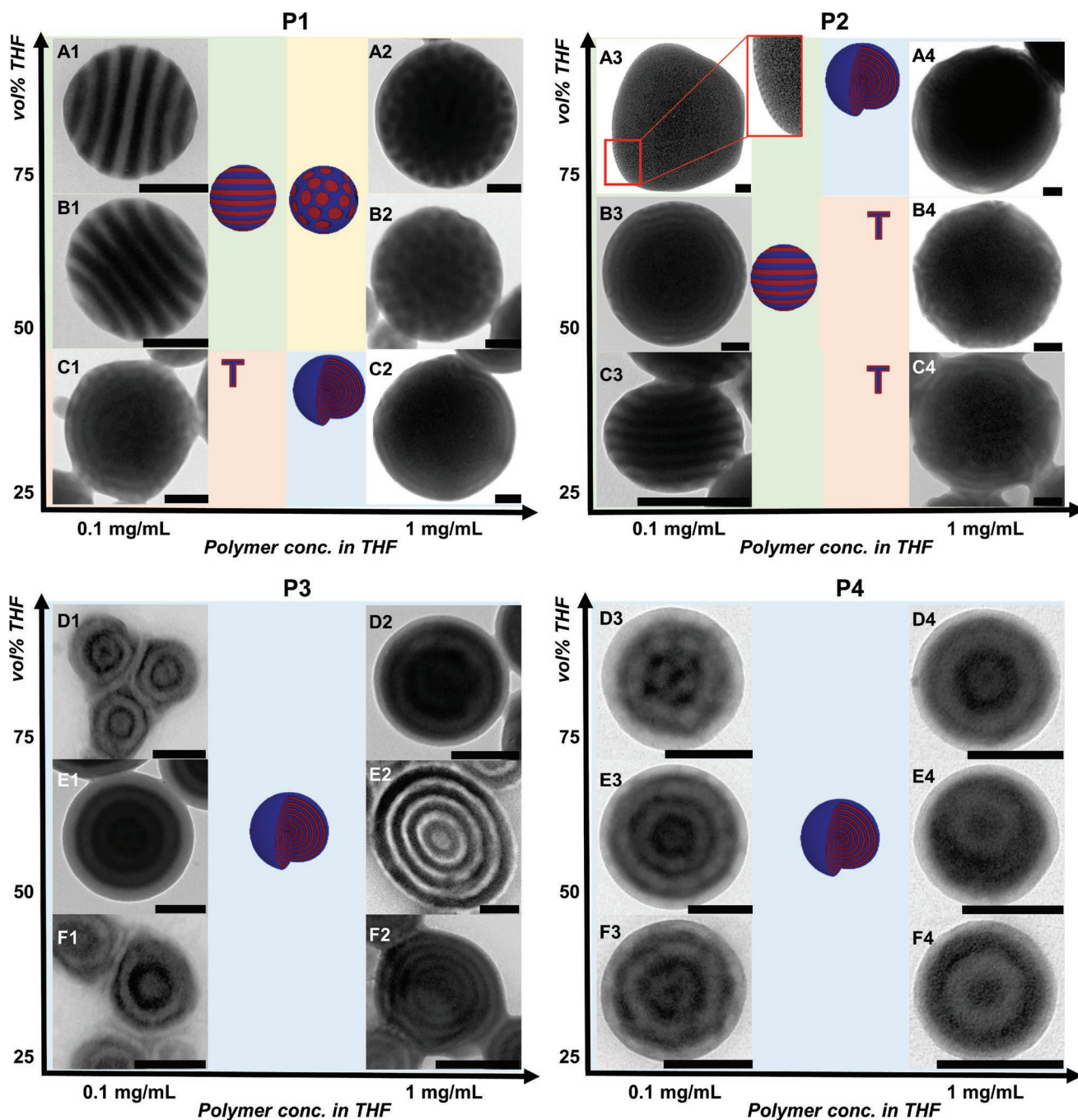


Figure 2. BF TEM images for nanoparticles obtained by nanoprecipitation with BCPs P1–4 in various conditions. E2 is a cross-sectional image of a nanoparticle. The dark regions represent the PI domains. All scale bars represent 100 nm. The blue and red domains in the schematic representations refer to the PS and PI blocks, respectively. “T” stands for transformation structures or disordered structures. Lower magnification TEM images displaying larger population of nanoparticles for each sample can be found in Figures S7–S9 in the Supporting Information.

to stacked lamellae are only observed at the lower polymer concentration of 0.1 mg mL^{-1} . Additionally, varying the amount of THF has an effect on the internal phase separation only in the case of P1 and P2, while P3 remains unperturbed. However, P3 does not form stacked lamellae structures under any of the conditions tested. Due to the hydrophobic nature of PFS, P3 precipitates quickly as soon as water is added (*vide supra*), while the presence of more polar chloro and azide groups in P1 and P2,

respectively, probably induces a slower precipitation, enhancing the formation of stacked lamellae structured nanoparticles. As P1 lies between P2 and P3 with respect to the hydrophilicity of the comonomer, such higher ordered structures form at 50 vol% and 75 vol% THF (Figure 2, A1 and B1), while they already appear at 25 vol% THF for P2 (Figure 2, C3). Apart from these observed phenomena, P2 shows distinct deviations from other polymers. Although at a concentration of 0.1 mg mL^{-1}

with 25 vol% THF (Figure 2, C3) **P2** forms clear stacked lamellae structured nanoparticles, such behavior becomes less apparent at 50 vol% and 75 vol% (Figure 2, B3 and A3). The internal structure of these increasingly larger particles is clearly not lamellar, yet a closer look at the surface of these nanoparticles reveals the presence of both P(S-co-AMS) and PI blocks (see Figure 2, A3 insert, as well as Figure S6, Supporting Information), allowing their surface structure to qualify as lamellae. There are clear interfacial effects, which are in analogy with those observed for sufficiently thick BCP thin films in which atmosphere-film and film-substrate interactions lead to differing phase organizations in the bulk and at the interfaces. In summary, the final morphologies are certainly the result of a complex interplay between relative swelling by THF, interfacial interactions with the continuously evolving THF/water mixture, concentration effects, global chain, and individual segment collapse kinetics, among others.

A constant observation is that in all cases where onion-like structures are encountered (Figure 2, C2, A4, and rows D–F), the outermost layer always consists of PS, as discerned by the light region that is unstained by osmium. Strikingly, this observation contradicts the fact that the lower interfacial surface tension between PI and water (55.8 mN m^{-1}) compared to that of PS and water (58 mN m^{-1}) would lead to formation of nanoparticles with PI as the outermost layer.^[46,47] The current observation is indeed the opposite of previously reported SORP results for PS-*b*-PI BCPs. Such a reversal in the interfacial behavior could arise from the presence of the carboxylic acid end group attached to the extremity of the PS block, which originates from the NMP initiator employed for the synthesis (see Scheme 2 and Scheme S1, Supporting Information). This highly polar moiety drives the formation of onion-like phase separated structures confining the PS block at the interface with the polar liquid phase. This hypothesis was confirmed by comparing the internal structure of nanoparticles produced by nanoprecipitation with the NMP-made PS-*b*-PI **P4**, which is devoid of functional comonomer unit, to those obtained in the same conditions with a commercial PS-*b*-PI BCP (**P5**), which was synthesized by anionic polymerization and bears no functional end or lateral group. As expected, in the latter case, onion-like structures were observed with PI as the outermost layer, as represented by the dark regions in Figure 3 and as opposed to Figure 2 (E3–4).

All mechanistic considerations set aside, it was possible to produce the targeted striped nanoparticles in the range of 150–300 nm from functional BCPs **P1** (Figure 2, A1 and B1)

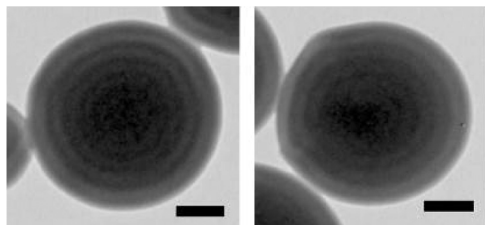


Figure 3. BF TEM images for nanoparticles obtained by nanoprecipitation with commercial BCP **P5**, at 50 vol% THF and a polymer concentration of 0.1 mg mL^{-1} (left) or 1 mg mL^{-1} (right). Dark regions represent PI domains, due to osmium staining. Scale bars represent 100 nm.

and **P2** (Figure 2, C3). However, under any of the applied conditions, **P3** did not form nanoparticles with stacked lamellae structures, yet rather onion-like structures with the PS phase constituting the outermost layer.

2.4. Effect on the Morphology of Phase Separation Using Block Copolymer Blends

From previous reports, it is known that mixing BCP blend systems can lead to a variety of phase separation morphologies.^[29] We thus assumed that blending **P3** with a well-chosen BCP could lead to the desired functional striped nanoparticles. As mentioned above, our custom-made BCPs obtained by NMP possess a carboxylic acid group at the end of the PS segment, which seems to drive this block towards the outside of onion-like structure. **P5** was chosen for two specific features: (i) similar molar mass and block volume fractions as in **P1–3** and (ii) its ability to undergo phase separation to form onion-structured nanoparticles where PI constitutes the outermost layer (Figure 3), unlike in **P3** where PS preferably forms the outermost layer. We hypothesize that when two such BCPs as **P3** and **P5** that form onion-like structures with opposite polymer segments at the interface are mixed, they would compete for the nanoparticle–water interface and lead to nanoparticles (equally) presenting both segments at the surface. Utilizing this concept, BCP blends were prepared using **P3** and **P5** (Table S4, blends 7–9, Supporting Information) in order to obtain nanoparticles exhibiting stacked lamellae internal structures. This was further extended to BCP blends of **P5** with **P1** and **P2** to better understand the transformation in internal phase separation structures. As both the functional BCPs **P1–3** and **P5** contain the same polymer segments, they should tend to precipitate together upon evaporation of THF leading to the formation of polymer blended nanoparticles. Since it was observed in the previous section that only lower polymer concentrations lead to striped particles, nanoparticles of BCP blends were prepared by mixing different weight ratios of each **P1–3** and **P5** at 0.1 mg mL^{-1} . The mixing ratio of THF:water for the nanoprecipitation was selected based on the condition that led to formation of nanoparticles with onion-like structures. Yet, as **P1** and **P2** do not form nanoparticles with clear onion-like structures, the closest conditions leading to such a structure, i.e., transformation from onion-like towards more ordered structure was chosen (Figure 2 C1 and B3, respectively for **P1** and **P2**). As discussed later, the chosen condition in case of **P1** additionally helps validating our hypothesis.

As expected, nanoparticles formed from BCP blends showed morphological transformations in the internal structure (Figure 4, B1–D1, B2–D2, and C3–D3) in comparison to BCP nanoparticles obtained from single BCPs (Figure 4, A1–A3 and E1–E3). For example, at 0.1 mg mL^{-1} and 75 vol% THF, both **P3** and **P5** independently formed nanoparticles exhibiting onion-like structures with an outermost layer composed of PS or PI (Figure 4, A3 or E3), respectively. Yet, when a 1:1 blend of **P3:P5** was prepared (Table S4, blend 8, Supporting Information), the nanoparticles formed by simultaneous precipitation and self-assembly of both BCPs featured stacked lamellae structures (Figure 4, C3, NP3). Similar transformation

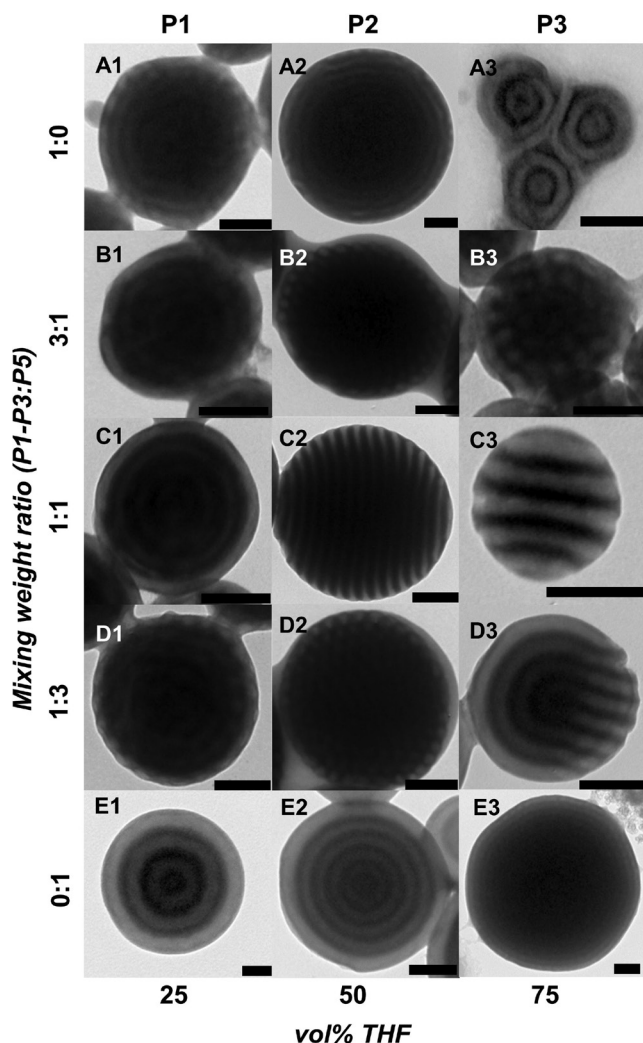


Figure 4. BF TEM images for nanoparticles obtained by nanoprecipitation with mixtures of custom-made BCPs **P1–3** and commercial BCP **P5**, at various weight ratios. THF contents of 25, 50, and 75 vol% were employed for blends with **P1**, **P2**, and **P3**, respectively. All scale bars represent 100 nm. Lower magnification TEM images displaying larger population of nanoparticles prepared from blends of **P1–3** with **P5** (here, rows B, C, and D) can be found in Figure S10 in the Supporting Information.

in the internal structures was evident on mixing **P2** with **P5** at a 1:1 weight ratio (Table S4, blend 4, Supporting Information and Figure 4, C2). It must be noted that in this case although **P2** does not independently form highly defined onion-like structures (Figure 2, B3), they constitute the bulk of the nanoparticle, while the surface displays a mixed PS/PI composition (Figure 4, A2 and Figure S6, Supporting Information). In this case, blending helps the stacked lamellar structure to form throughout the entire particles. It is interesting to note that such transformation in the internal structures only holds true for specific mixing ratios. Indeed, other blends of **P2** (3:1 and 1:3; Figure 4, B2 and D2) or **P3** (3:1 and 1:3; Figure 4, B3 and D3) with **P5** did not lead to pure stacked lamellae structures. Mixing **P1** in conditions where it does not form onion-like structures with PS on the outside (Figure 4, A1) together with **P5** (Figure 4, E1) does not produce blend nanoparticles with the

desired striped morphology (Figure 4, B1–D1), which validates this hypothesis.

The current set of blends is the first example of nanoparticles made by mixing AB BCPs with A'B counterparts. In spite of the difficulty to extract clear trends, this set of blends shows the influence of functional moieties in driving the transformation of internal structures, since mixing BCPs based essentially on the same motifs, yet differing by a small fraction of functional moieties, leads to a range of well-defined morphologies and their intermediate states. The clearest case is here that of **P3**, where in the present conditions, it undergoes morphological changes with increasing addition of **P5**: (i) pure **P3** gives onion-like structures with PS outside; (ii) at 25 wt% of **P5**, a spherical internal morphology is obtained; (iii) at 50 wt%, striped particles are produced; and (iv) at 75 wt%, a transformation state between a striped morphology and an onion-like structure with PI outside is observed.

Using the blending method, nanoparticles **NP3** containing BCP **P3** with the desired striped morphology could thus be obtained (Figure 4, C3). A model to study PS-*b*-PI BCPs confined in 3D space results in an understanding morphologies of phase separation depending on the model parameters.^[48] Consequently, to gain deeper insights in the exact composition of the phases present in the internal structures of **NP3**, electron tomography was performed in order to reconstruct a 3D model. For this, TEM images were taken by tilting the sample grid from -60 to $+60^\circ$ with 1° increments. In the half-cut 3D reconstructed image, the exact volumes of both PS and PI, represented by blue and green, respectively, can be envisaged (Figure S11, Supporting Information). The PS and PI phases distinctly form alternate stacks with regular periods, both internally and at the surface of the nanoparticle, which correlates with the 2D images of the phase-separated nanoparticles obtained by experimental methods.

2.5. Site-Specific Functionalization of Reactive Patchy Nanoparticles

Having successfully obtained functional stacked lamellae nanoparticles that have both PI and functional PS segments on the surface for each functional BCP, the availability of the functional groups for further immobilization of molecules was investigated. Here, as a first example of postfunctionalization of reactive patchy nanoparticles obtained by nanoprecipitation, we demonstrate the modification of pentafluorophenylalkyl nanoparticles **NP3** by so-called *para*-fluoro–thiol reaction (PFTR)^[49] using cysteine (Figure 5A). Notably, we recently demonstrated the feasibility of this reaction in an aqueous environment at basic pH.^[50] Cysteine was chosen as the thiol reactant for PFTR with **NP3** for the following reasons: (i) it is a water-soluble amino acid; (ii) as it is a small molecule, the sulfur atoms can be precisely mapped by energy dispersive X-ray detector (EDX) to prove the patterned immobilization only in the PS segment; and (iii) its ionizable nature enables clear assessment using zeta potential measurements. **NP3** nanoparticles were incubated with cysteine at pH = 13.0, where thiol deprotonation occurs and leads to reaction at the *para* position of the pentafluorophenyl moiety.

STEM in combination with EDX mapping was used to investigate the morphology and the atomic composition of the reacted

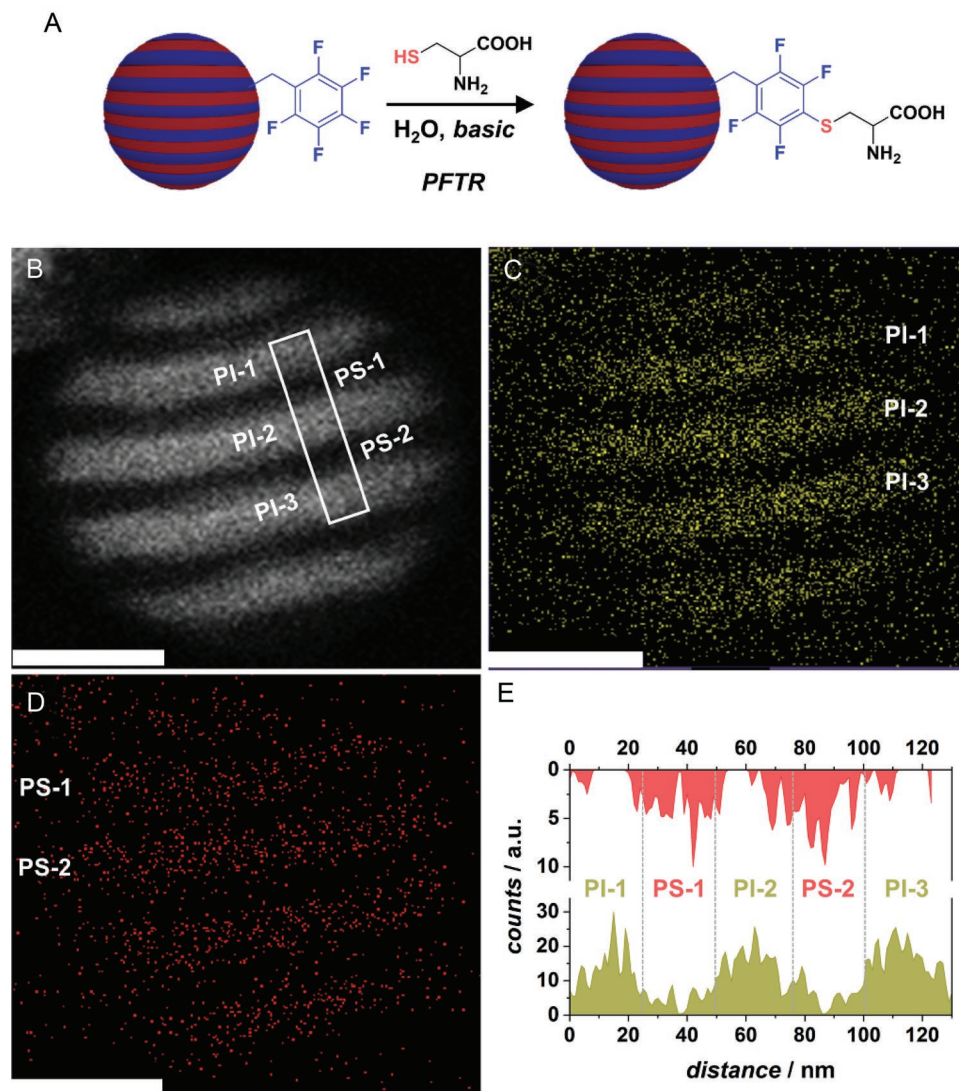


Figure 5. A) Schematic representation of PFTR on the PS segment of the striped nanoparticles **NP3** with cysteine. B) DF STEM image of **NP3** nanoparticles where the bright parts (PI-1–3) represent the PI segment, while the dark regions that of PS. C) EDX mapping of Os- $L\alpha$ lines represented by green dots. D) EDX mapping of S- $K\alpha$ lines represented by red dots. E) Grey value pixel map obtained by integrating the area in the marked region in part (B) showing PS segments PS-1–2 and PI segments PI-1–3 showing alternate stacks of S (red) and Os (green) that represent PS and PI segments, respectively. All scale bars represent 50 nm.

nanoparticles. Figure 5B represents a DF STEM image of **NP3**, where the bright and dark parts represent the PI domains (marked as PI-1 to PI-3) and PS domains (PS-1 and PS-2), respectively. Figure 5C shows the corresponding map of dissipative energy matching the Os- $L\alpha$ line. As expected, it faithfully reproduces the PI domains PI-1 to PI-3, which were selectively stained and crosslinked by osmium tetroxide. Figure 5D is another dissipative energy map of the same region of the sample, yet indexed to the S- $K\alpha$ line. A new stripe pattern is clearly observed, in alternate stacks compared to Figure 5C and reproducing the dark domains of the particle in Figure 5B. By tracing a line perpendicular to the domains and plotting the intensities obtained from both energy maps (Figure 5B), a clear alternation of osmium- and sulfur-containing domains is visible (Figure 5E). This unambiguously proves the success of the PFTR reaction, hence the presence of

the pentafluorophenyl units at the surface of the particles, as well as the site-selective incorporation of sulfur-containing species at the surface of the PS domains. Additionally, an EDX spectrum of **NP3** shows the presence of both Os and S confirming the reaction (Figure S12, Supporting Information).

Furthermore, to confirm the presence of cysteine at the surface of the nanoparticles, zeta potential measurements carried out in water (pH = 7). Significantly negative zeta potential values were recorded for the original, non-reacted **NP3** nanoparticles and a control sample (−20.3 and −24.1 mV, respectively), while **NP3** after PFTR with cysteine exhibited a zeta potential value of +0.018 mV. The original negative value arises from the presence of the carboxylic acid end groups at the PS end of the constituting BCP **P3**. The positive value obtained after PFTR is a strong indication of the effective grafting of an amphiphilic

amino acid such as cysteine on the surface of the nanoparticles. All the above measurements prove that nanoparticles prepared by nanoprecipitation with functional BCPs can be precisely patterned with specific molecules for potential applications.

2.6. Synthesis and Surface Functionalization of Nanodiscs

STEM and ET images of striped particles strongly support the formation of unidirectionally stacked lamellar structures throughout the entire striped particles. Within the PI domains, OsO_4 was reacted with the double bonds to stain and crosslink. In a previous report, Higuchi et al. described a so-called *selective immobilization and selective elution* (SISE) method to produce nanodiscs from stacked lamellae structured nanoparticles.^[8] This technique proceeds by swelling with good solvent multicompartiment particles which were selectively crosslinked in one domain. We have used the same SISE method to fabricate surface-reactive nanodiscs **ND3** from OsO_4 -crosslinked **NP3**. The latter were incubated in THF and sonicated in order to fully swell and disentangle the PS domains, leading to a process akin to delamination or exfoliation of the PI stacks. These nanodiscs thus consist of an osmium-crosslinked disc-shaped PI core and a pentafluorophenylalkyl-functionalized brush-like PS shell. **Figure 6A–C** illustrates the SISE-based transformation: STEM evidences the presence of flat, circular objects with diameters in the range of those of the original **NP3** nanoparticles and below. **ND3** nanodiscs were found to be ≈ 18 nm in thickness by atomic force microscopy (AFM), which corresponds well to the thickness of a stack of PS or PI in **NP3** nanoparticles (**Figure 6C**). As the PS block of **P3** contains pentafluorophenyl moieties, **ND3** can then further be reacted with thiol-containing molecules to obtain surface functional nanodiscs.

In order to demonstrate the surface reactivity of the nanodiscs **ND3** and simultaneously showcase the versatility of PFTR for the site-specific functionalization of nanostructures, we sought to employ another thiol than cysteine. A short polyethylene glycol-bearing thiol and fluorescein groups at either of its ends (FITC-PEG-SH) was used for further characterization by high-resolution fluorescence microscopy. After PFTR, stimulated emission depletion (STED) microscopy revealed objects with a green fluorescent halo and a dark central core, proving the attachment of FITC-PEG-SH at the surface of the nanodiscs (**Figure 6D**). It is assumed that the surface of the nanodiscs consists of P(*S-co*-PFS) layers that are so dense that only the peripheral sites, owing to radial spreading of the chains, are accessible to a small polymer like FITC-PEG-SH. To prove that the thiol was not non-specifically adsorbed on the surface, a control reaction was performed, wherein the nanodiscs **ND3** were incubated with the thiol in the absence of the base catalyst. In this case, particles detected using the BF mode of the microscope did not display any fluorescence in STED mode (see **Figure S13**, Supporting Information).

3. Conclusion

Three different functional analogues of PS-*b*-PI with equal volume fractions and bearing a small amount of reactive

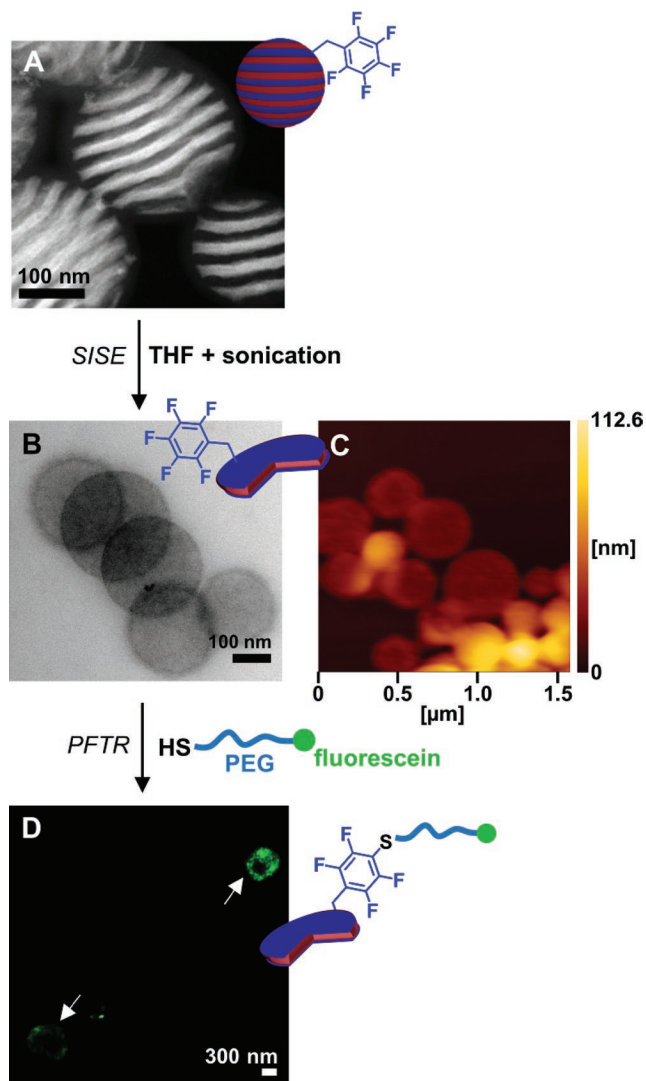


Figure 6. A, B) DF STEM images of nanoparticles **NP3** with stacked lamellae structures and the corresponding nanodiscs **ND3** obtained by SISE. C) AFM topography image of the nanodiscs **ND3**. D) STED fluorescence microscopy image of **ND3** after PFTR with FITC-PEG-SH.

moieties (i.e., halide, azide, or pentafluoroalkyl) were synthesized by NMP. Formation of nanoparticles by simple nanoprecipitation consistently led to nanoparticles with internal phase separation, whose exact nature depended on the nature of the reactive groups. The encountered morphologies ranged from onion-like to dotted or stacked lamellar patterns. Intermediate transformation structures were also found, in the absence of annealing. The onion-like structures systematically displayed an external PS-based layer due to the presence of a carboxylic acid group arising from the polymerization initiator at the PS chain end. When targeted striped morphologies could not be attained from the BCP alone, blending with a non-functional PS-*b*-PI copolymer was successfully applied, exploiting an interfacial competing phenomenon. As an example, site-selective surface functionalization of the pentafluoroalkyl-functionalized striped particles was achieved by aqueous *para*-fluoro-thiol reaction, as evidenced by SEM/EDX mapping. Furthermore,

these same nanoparticles, once crosslinked in the PI domain, were used to produce by selective delamination surface-reactive nanodiscs exhibiting surface reactivity, as demonstrated by STED microscopy.

Nanoprecipitation and tandem internal phase separation of functional BCPs is a powerful, yet simple method to produce functional nanostructured nano-objects bringing us one step closer to interfacial mimics of natural nanoparticles, and as such, may give access to interesting materials for fundamental biological studies or biotechnological uses. Notably, the well-ordered domains of striped particles could be employed for controlled co-enzyme immobilization to produce biosensors.^[51] The nanodiscs may have particular interfacial properties at liquid–liquid interfaces but also with biological membranes. Such flat anisotropic disc-like nanostructures are rather rare in the synthetic realm,^[52] yet a famous example in the biological context is that of phospholipid/membrane protein co-assembly.^[53] Further research should be dealing with corresponding patterned immobilization of biomolecular modules, as well as expanding the method to other kind of polymers, such as biocompatible or (bio)degradable counterparts. Also investigating other patch geometries would be useful in the area of supracolloidal assemblies.^[16,17]

4. Experimental Section

Details concerning materials as well as macromolecular synthesis and characterization can be found in the Supporting Information file.

Dynamic Light Scattering: Measurements were performed on a Malvern Zetasizer Nano ZS that uses NIBS (non-invasive backscattering) to measure the hydrodynamic diameter of the nanoparticles. The zeta potential was also measured using the same instrument in deionized water. Measurements were performed after full evaporation of THF.

(Scanning) Transmission Electron Microscopy: The nanodiscs were measured on a JEOL-2100F high-resolution STEM with Cs-corrector instrument at 200 KeV accelerating voltage attached to a high angle annular dark field detector. A JS single-tilt holder was used to mount the grid. The instrument had an EDX module attached for elemental analysis: The nanoparticles were either measured using the above STEM or a TEM (H-7650, Hitachi, Japan) set to an accelerating voltage of 100 kV attached to a BF detector. For statistical analysis (mean diameter and polydispersity), about 100 particles were listed and manually measured on electron micrographs using ImageJ “analyze particle” mode.

Electron Tomography (ET): 3D structures of striped particle were reconstructed by using the series of TEM images observed with an acceleration voltage of 100 kV. The series of TEM images were acquired at tilt angles from -60° to $+60^\circ$ in 1° steps. The TEM images were aligned and reconstructed using an imaging software (Image J, NIH) with a “Tomo-J” plug-in.^[54] The reconstruction was performed by using the weighted backprojection algorithm. The reconstructed images were refined and colored with an imaging software (Cinema 4D, MAXON, Inc.).

Atomic Force Microscopy: One drop of THF dispersion of nanodiscs was cast on a Si substrate and dried at room temperature. Surface structures of the nanodiscs were then measured by AFM, SPI400, SII using the DFM (tapping) mode.

Stimulated Emission Depletion Microscopy: The fluorescent nanodiscs were characterized with a Leica TCS SP8 Laser Scanning Confocal Microscope. Excitation was with a white light laser set to 488 nm. The Hybrid Detector window was set to capture 500–550 nm, gated at 1.5–6.5 ns. The STED super-resolution imaging was carried out with a 592 nm depletion laser. Postimage acquisition deconvolution was performed with Huygens Professional.

Preparation of Nanoparticles: The BCPs were dissolved in THF at a concentration of 1.0 and 0.1 mg mL⁻¹. The nanoparticles were prepared using a nanoprecipitation method (Scheme 2), as previously reported by Yabu et al.,^[33] using various THF:water ratios (Table S3, Supporting Information). More precisely, 1.5, 1, or 0.5 mL of millipore water were added dropwise at the rate of 1 mL min⁻¹ into 0.5, 1, or 1.5 mL of the polymer solution in THF, respectively, with vigorous stirring. THF was then allowed to evaporate at room temperature and atmospheric pressure for 4 d. The size of all nanoparticles was measured by DLS, as summarized in Table S3 in the Supporting Information. In another set of experiments, to study the transformation of internal structures with BCP blends, the polymers **P1–3** were mixed in various ratios with the commercial, non-functional PS-*b*-PI BCP **P5**. The nanoparticles prepared using these blends are described in Table S4 in the Supporting Information.

Observation of Phase-Separated Structures in the Nanoparticles: After nanoprecipitation, it was made sure that the THF was completely evaporated. Following this, the nanoparticle dispersion in water obtained by nanoprecipitation was thoroughly sonicated for 5 min and 0.5 mL of it was transferred into an Eppendorf tube. The nanoparticles were stained by mixing with 0.5 mL of a 0.2 vol% solution of OsO₄ for 2 h. Excess OsO₄ was washed away by ultracentrifugation of the stained nanoparticles (Hitachi, himac CF16RX, 12000 rpm, 15 min, 5 °C). The pellet was collected, redispersed in 700 μL millipore water, and ultrasonicated for 5 min to obtain a homogeneously dispersed nanoparticle solution. This washing process was repeated four times and the pellet was finally redispersed in water to obtain OsO₄-stained nanoparticles. A Cu grid with a carbon-coated membrane was subjected to UV/O₃ treatment (Iwasaki, Japan) for 3 min to render its surface hydrophilic and a drop of the stained nanoparticles was then casted onto it. After drying in air, the sample was observed using TEM (BF) and in some cases STEM (DF).

Preparation of Functional Nanodiscs from Osmium-Crosslinked Nanoparticles: Functional BCP nanoparticles **NP3** that exhibit stacked lamellae patterns with pentafluorophenyl-functionalized PS domains (Blend 8, Figure 4 C3, and Table S4, Supporting Information) were used in this experiment to prepare functional nanodiscs **ND3**. This was achieved by following a method previously described by Higuchi et al. as SISE.^[8] For this, first a 200 μL dispersion of the nanoprecipitation-made nanoparticles **NP3** was stained with osmium tetroxide as described above. After washing thoroughly, the final pellet was redispersed in 700 μL THF and sonicated at room temperature for 5 h. A 2 μL suspension was casted on a Cu grid coated with carbon for STEM analysis.

Reaction on Functional BCP Nanoparticles: To prove the reactivity of the functional groups on the surface of the functional nanoparticles and nanodiscs, striped particles **NP3** and nanodiscs **ND3** both containing pentafluorophenyl units were chosen to perform PFTR. In the case of **NP3**, a 100 μL homogeneous suspension of **NP3** in water was placed in an Eppendorf tube. To this, 2 mL of 10 mg mL⁻¹ cysteine in pH 13 buffer was added and the solution was incubated in a shaker at 50 °C for 16 h. On the other hand, for **ND3**, this reaction was performed in THF. To 100 μL of the nanodisc dispersion, first 2 μL of DBU followed by 1 mL of 10 mg mL⁻¹ of FITC-PEG-SH was added and the solution was placed in a shaker overnight at room temperature. To prove that the thiols do not non-specifically adsorb on the surface of the nanoparticles or nanodiscs, control experiments were performed. The **NP3** and **ND3** control samples were incubated under the same conditions as the reaction sample, but in the absence of the catalyst, i.e., in neutral water instead of pH 13 buffer solution for **NP3** and in THF in the absence of DBU for **ND3**. After the reactions, in order to remove the buffer solution/DBU and cysteine/FITC-PEG-SH, the solution was centrifuged (15 000 rpm, 30 min, 5 °C), the supernatant carefully decanted and the pellet washed with 1 mL 0.01% Tween20 solution. This washing step was repeated thrice and finally once with deionized water to remove any excess reactants. The final pellet was redispersed in 700 μL of deionized water, tip sonicated, and casted on a copper grid coated with carbon for STEM or on a microscopy glass slide for STED analysis.

Supporting Information

Supporting Information is available from the Wiley Online Library or from the author.

Acknowledgements

The authors would like to thank the German Federal Ministry of Education and Research (BMBF) for the current funding in the frame of Molecular Interaction Engineering program (Biotechnologie 2020+, Grant No. 031A095C). D.V. and H.Y. are grateful to Minori Suzuki for providing training and assistance with TEM. The authors are also thankful to the “Michigan Center for Materials Characterization” and its staff assistance (Bobby Kerns, Kai Sun, and Haiping Sun) for the use of JEOL 2100-F STEM. D.V. also thanks Linda Barthel and UMich Microscopy and Image Analysis for the STED microscopy measurements. H.Y. would like to thank KAKENHI (Nos. 17H01223 and 16K14071), Japan for financial support, respectively. Finally, Prof. Barner-Kowollik (QUT and ITCP, KIT) is thanked for his constant support.

Conflict of Interest

The authors declare no conflict of interest.

Keywords

functional block copolymers, morphology control, nanodiscs, nanoparticles, *para*-fluoro–thiol reaction

Received: February 1, 2018

Revised: May 20, 2018

Published online: August 10, 2018

- [1] A. H. Gröschel, A. Walther, T. I. Löbling, F. H. Schacher, H. Schmalz, A. H. E. Müller, *Nature* **2013**, *503*, 247.
- [2] D. Klinger, C. X. Wang, L. A. Connal, D. J. Audus, S. G. Jang, S. Kraemer, K. L. Killops, G. H. Fredrickson, E. J. Kramer, C. J. Hawker, *Angew. Chem., Int. Ed.* **2014**, *53*, 7018.
- [3] C. V. Synatschke, T. Nomoto, H. Cabral, M. Förtsch, K. Toh, Y. Matsumoto, K. Miyazaki, A. Hanisch, F. H. Schacher, A. Kishimura, N. Nishiyama, A. H. E. Müller, K. Kataoka, *ACS Nano* **2014**, *8*, 1161.
- [4] S. Zhang, H.-J. Sun, A. D. Hughes, R.-O. Moussodia, A. Bertin, Y. Chen, D. J. Pochan, P. A. Heiney, M. L. Klein, V. Percec, *Proc. Natl. Acad. Sci. USA* **2014**, *111*, 9058 LP.
- [5] S. Ravaine, E. Duguet, *Curr. Opin. Colloid Interface Sci.* **2017**, *30*, 45.
- [6] T. Higuchi, A. Tajima, H. Yabu, M. Shimomura, *Soft Matter* **2008**, *4*, 1302.
- [7] H. Yabu, M. Kanahara, M. Shimomura, T. Arita, K. Harano, E. Nakamura, T. Higuchi, H. Jinnai, *ACS Appl. Mater. Interfaces* **2013**, *5*, 3262.
- [8] T. Higuchi, A. Tajima, K. Motoyoshi, H. Yabu, M. Shimomura, *Angew. Chem., Int. Ed.* **2009**, *48*, 5125.
- [9] S. G. Jang, D. J. Audus, D. Klinger, D. V. Krogstad, B. J. Kim, A. Cameron, S.-W. Kim, K. T. Delaney, S.-M. Hur, K. L. Killops, G. H. Fredrickson, E. J. Kramer, C. J. Hawker, *J. Am. Chem. Soc.* **2013**, *135*, 6649.
- [10] J. M. Shin, Y. Kim, H. Yun, G.-R. Yi, B. J. Kim, *ACS Nano* **2017**, *11*, 2133.
- [11] W. Zhang, Z. Kochovski, Y. Lu, B. V. K. J. Schmidt, M. Antonietti, J. Yuan, *ACS Nano* **2016**, *10*, 7731.
- [12] S.-J. Jeon, G.-R. Yi, S.-M. Yang, *Adv. Mater.* **2008**, *20*, 4103.
- [13] S.-J. Jeon, G.-R. Yi, C. M. Koo, S.-M. Yang, *Macromolecules* **2007**, *40*, 8430.
- [14] D. Klinger, M. J. Robb, J. M. Spruell, N. A. Lynd, C. J. Hawker, L. A. Connal, *Polym. Chem.* **2013**, *4*, 5038.
- [15] M. Okubo, N. Saito, R. Takekoh, H. Kobayashi, *Polymer* **2005**, *46*, 1151.
- [16] S. C. Glotzer, M. J. Solomon, *Nat. Mater.* **2007**, *6*, 557.
- [17] É. Duguet, C. Hubert, C. Chomette, A. Perro, S. Ravaine, *Comptes Rendus Chim.* **2016**, *19*, 173.
- [18] J. Du, R. K. O'Reilly, *Chem. Soc. Rev.* **2011**, *40*, 2402.
- [19] K. J. Lee, J. Yoon, J. Lahann, *Curr. Opin. Colloid Interface Sci.* **2011**, *16*, 195.
- [20] A. Walther, A. H. E. Müller, *Chem. Rev.* **2013**, *113*, 5194.
- [21] D. J. Lunn, J. R. Finnegan, I. Manners, *Chem. Sci.* **2015**, *6*, 3663.
- [22] S. Schoffelen, J. C. M. van Hest, *Curr. Opin. Struct. Biol.* **2013**, *23*, 613.
- [23] A. Verma, O. Uzun, Y. Hu, Y. Hu, H.-S. Han, N. Watson, S. Chen, D. J. Irvine, F. Stellacci, *Nat. Mater.* **2008**, *7*, 588.
- [24] Z. Poon, S. Ch: en, A. C. Engler, H. Lee, E. Atas, G. von Maltzahn, S. N. Bhatia, P. T. Hammond, *Angew. Chem., Int. Ed.* **2010**, *49*, 7266.
- [25] M. Massignani, C. LoPresti, A. Blanz, J. Madsen, S. P. Armes, A. L. Lewis, G. Battaglia, *Small* **2009**, *5*, 2424.
- [26] A. Akinc, G. Battaglia, *Cold Spring Harbor Perspect. Biol.* **2013**, *5*, a016980.
- [27] R. Deng, F. Liang, W. Li, S. Liu, R. Liang, M. Cai, Z. Yang, J. Zhu, *Small* **2013**, *9*, 4099.
- [28] T. Higuchi, A. Tajima, K. Motoyoshi, H. Yabu, M. Shimomura, *Angew. Chem., Int. Ed.* **2008**, *47*, 8044.
- [29] H. Yabu, K. Motoyoshi, T. Higuchi, M. Shimomura, *Phys. Chem. Chem. Phys.* **2010**, *12*, 11944.
- [30] M. J. Robb, L. A. Connal, B. F. Lee, N. A. Lynd, C. J. Hawker, *Polym. Chem.* **2012**, *3*, 1618.
- [31] Y. Hirai, T. Wakiya, H. Yabu, *Polym. Chem.* **2017**, *8*, 1754.
- [32] B. V. K. J. Schmidt, C. X. Wang, S. Kraemer, L. A. Connal, D. Klinger, *Polym. Chem.* **2018**, *9*, 1638.
- [33] H. Yabu, T. Higuchi, M. Shimomura, *Adv. Mater.* **2005**, *17*, 2062.
- [34] H. Turgut, N. Dingenouts, V. Trouillet, P. Krolla-Sidenstein, H. Gliemann, G. Delaitre, *unpublished*.
- [35] F. S. Bates, G. H. Fredrickson, *Phys. Today* **1999**, *52*, 32.
- [36] S. Egli, H. Schlaad, N. Bruns, W. Meier, *Polymers* **2011**, *3*, 252.
- [37] I. Wyman, G. Njikang, G. Liu, *Prog. Polym. Sci.* **2011**, *36*, 1152.
- [38] Z. Jin, H. Fan, *Soft Matter* **2014**, *10*, 9212.
- [39] C. A. Vaine, M. K. Patel, J. Zhu, E. Lee, R. W. Finberg, R. C. Hayward, E. A. Kurt-Jones, *J. Immunol.* **2013**, *190*, 3525 LP.
- [40] K. Yang, Y.-Q. Ma, *Nat. Nanotechnol.* **2010**, *5*, 579.
- [41] H. Yabu, T. Higuchi, K. Ijro, M. Shimomura, *Chaos* **2005**, *15*, 47505.
- [42] M. Pinna, X. Guo, A. V. Zvelindovsky, *Polymer* **2008**, *49*, 2797.
- [43] B. Yu, B. Li, Q. Jin, D. Ding, A.-C. Shi, *Macromolecules* **2007**, *40*, 9133.
- [44] K. Motoyoshi, A. Tajima, T. Higuchi, H. Yabu, M. Shimomura, *Soft Matter* **2010**, *6*, 1253.
- [45] L. Li, K. Matsunaga, J. Zhu, T. Higuchi, H. Yabu, M. Shimomura, H. Jinnai, R. C. Hayward, T. P. Russell, *Macromolecules* **2010**, *43*, 7807.
- [46] T. Higuchi, K. Motoyoshi, H. Sugimori, H. Jinnai, H. Yabu, M. Shimomura, *Macromol. Rapid Commun.* **2010**, *31*, 1773.
- [47] E. Avalos, T. Teramoto, H. Komiyama, H. Yabu, Y. Nishiura, *ACS Omega* **2018**, *3*, 1304.
- [48] E. Avalos, T. Higuchi, T. Teramoto, H. Yabu, Y. Nishiura, *Soft Matter* **2016**, *12*, 5905.
- [49] G. Delaitre, L. Barner, *Polym. Chem.* **2018**, *9*, 2679.
- [50] H. Turgut, A. C. Schmidt, P. Wadhvani, A. Welle, R. Müller, G. Delaitre, *Polym. Chem.* **2017**, *8*, 1288.
- [51] F. Kazenwadel, M. Franzreb, B. E. Rapp, *Anal. Methods* **2015**, *7*, 4030.
- [52] X. Qu, L. Omar, T. B. H. Le, L. Tetley, K. Bolton, K. W. Chooi, W. Wang, I. F. Uchebgu, *Langmuir* **2008**, *24*, 9997.
- [53] T. H. Bayburt, S. G. Sligar, *FEBS Lett.* **2010**, *584*, 1721.
- [54] C. Messaoudil, T. Boudier, C. O. S. Sorzano, S. Marco, *BMC Bioinformatics* **2007**, *8*, 288.